Site Diversity in Downlink Optical Satellite Networks Through Ground Station Selection

EYLEM ERDOGAN[ID][1]**, (Senior Member, IEEE), IBRAHIM ALTUNBAS**[ID][2]**, (Senior Member, IEEE), GUNES KARABULUT KURT**[ID][2,4]**, (Senior Member, IEEE), MICHEL BELLEMARE**[3]**, GUILLAUME LAMONTAGNE**[3]**, AND HALIM YANIKOMEROGLU**[ID][4]**, (Fellow, IEEE)**

[1]Department of Electrical and Electronics Engineering, Istanbul Medeniyet University, 34700 Istanbul, Turkey
[2]Electronics and Communication Engineering Department, Istanbul Technical University, 34469 Maslak, Turkey
[3]Satellite Systems, MDA, Sainte-Anne-de-Bellevue, QC H9X 3R2, Canada
[4]Department of Systems and Computer Engineering, Carleton University, Ottawa, ON K1S 5B6, Canada

Corresponding author: Eylem Erdogan (eylem.erdogan@medeniyet.edu.tr)

ABSTRACT Recent advances have shown that satellite communication (SatCom) will be an important enabler for next generation terrestrial networks as it can provide numerous advantages, including global coverage, high speed connectivity, reliability, and instant deployment. An ideal alternative for radio frequency (RF) satellites is its free-space optical (FSO) counterpart. FSO or laser SatCom can mitigate the problems occurring in RF SatCom, while providing important advantages, including reduced mass, lower consumption, better throughput, and lower costs. Furthermore, laser SatCom is inherently resistant to jamming, interception, and interference. Owing to these benefits, this paper focuses on downlink laser SatCom, where the best ground station (GS) is selected among numerous candidates to provide reliable connectivity and site diversity. To quantify the performance of the proposed scheme, we derive closed-form outage probability and ergodic capacity expressions for two different practical GS deployment scenarios. Thereafter, asymptotic analysis is conducted to obtain the overall site diversity order, and aperture averaging is studied to illustrate the impact of aperture diameter on the overall performance. Furthermore, we investigate the site diversity order for a constellation of satellites that are communicating with the best GS by using opportunistic scheduling. Finally, important design guidelines that can be useful in the design of practical laser SatComs are outlined.

INDEX TERMS Laser satellite communication, site diversity, free-space optical communication, atmospheric turbulence and attenuation.

I. INTRODUCTION

Satellite communication (SatCom) has become an important part of aerial networks in recent years due to its capabilities, which include flawless wireless connectivity, wide service coverage, and high-fidelity services for all the users around the world. An important feature of SatCom is to simultaneously transfer the signal rapidly around the Earth by providing distance-insensitive point-to-multipoint communications [1]. So far, satellites have been used for television coverage, data communication, navigation, weather forecasts, climate and environmental monitoring, space science, and so on [2]. Satellites can be divided into three main categories depending

The associate editor coordinating the review of this manuscript and approving it for publication was Nan Wu[ID].

on their altitudes and orbit types, low Earth orbit (LEO), medium Earth orbit (MEO) and geostationary Earth orbit (GEO). GEO satellites are located at about 36000 km above the Earth's equator to provide wide coverage, whereas LEO satellites, which circle around the Earth at lower altitudes, have faster rotations, require less power, and are cheaper than GEO and MEO satellites [3]. The technology behind SatCom is mainly based on radio-frequency (RF) systems, where 100 MHz to 50 GHz frequencies are used depending on the types and applications of satellites. In recent years, SatCom has emerged to provide high-speed, seamless broadband Internet connectivity around the globe as many different companies have started to launch constellations of satellites. For instance, SpaceX's Starlink recently began launching LEO satellites operating at high frequencies [4].

Similarly, OneWeb has launched about 104 LEO satellites in 2020, which operate in the K_a-K_u band of the frequency spectrum [5]. These recent developments suggest that RF-SatCom will become a key enabler in the integration of aerial and terrestrial networks in future wireless communication systems. In RF-SatCom, the most important drawbacks are cost, regulatory restrictions and limited available bandwidth, as it requires high data rates and broader bandwidths to connect anyone at anytime. Furthermore, RF-SatCom is prone to interference, jamming, and interception, which pose security risks, especially for military communications.

As a solution to these problems, free-space optical (FSO) or laser SatCom has attracted considerable interest both in recent academic and industry publications [6]. In laser SatCom, 20 to 375 THz spectrum[1] can be used to provide very high throughput in satellite-to-ground (downlink) and ground-to-satellite (uplink) communications [7]. Laser SatCom can also provide significant advantages compared to its RF counterpart, including smaller antennas, reduced mass, lower consumption, better throughput, and lower costs. Furthermore, the narrow beam used in optical systems can provide secure communication, and it is immune to jamming, interception, interference. In addition, laser SatCom does not require a spectrum operating license for frequency use due to its inherent nature [8]. Due to these advantages, laser SatCom is expected to become a key enabler for future optical satellite systems, particularly for satellite-to-ground (downlink) communications, where line-of-sight (LOS) connectivity can be established perfectly [9]. In downlink laser SatCom, the major adverse effects are atmospheric turbulence, atmospheric attenuation, and angle of arrival (AoA) fluctuations [7]. The latter can be attenuated by using variable-focus lenses, which can adjust the beam size [10]. Also, aperture averaging, where the scintillation is spatially averaged over the aperture, can be used to reduce the adverse effects of atmospheric turbulence [11]. Finally, atmospheric attenuation due to adverse weather conditions can be resolved by achieving site diversity, in which the number of optical links can be enhanced by using multiple ground stations [12]–[15]. It can also be resolved by attaining spatial diversity with the aid of multiple apertures on a single GS, using appropriate combining techniques, such as selection combining, maximum ratio combining or equal gain combining [16], [17].

Due to the advantages outlined above, optical satellites have become an important topic in the recent literature. In [18]–[21], the issue of optical ground-to-satellite (uplink) communication was considered, and important performance metrics, including outage probability, error probability, and link capacity, were obtained in the presence beam wandering, climatic effects, and atmospheric attenuation. By contrast, [16] and [22] focused on downlink SatCom, where the former investigated the impact of spatial diversity and

aperture averaging, and the latter examined the throughput. Furthermore, [23] and [24] proposed using FSO communication as a feeder link where the ground station (GS) feeds the satellite through a high capacity link.

In this paper, we pursue a different line of inquiry by providing a detailed analysis for the downlink optical SatCom systems. More precisely, to deal with the adverse weather conditions, we try to maximize the site diversity by selecting the best GS that provides the best channel conditions. It is important to note that site diversity, which can be crucial for creating seamless connectivity between satellite-to-ground links, has already been discussed in the literature e.g., [12]–[15] and the references therein. However, these previous works focused on the optimum GS selection problem from the network layer point-of-view. To the best of our knowledge, none of these works have considered the physical layer performance of the optical SatCom with GS selection. Given the importance of site diversity, and to fill the gap in the literature, we focus on the physical layer performance of the downlink optical SatCom with multiple GSs.[2] To quantify the performance of the proposed setup, we consider an aggregate channel model consisting of atmospheric turbulence and atmospheric attenuation, where we obtained two performance indicators, outage probability and ergodic capacity. We also consider the scenario of a constellation of satellites in which the best satellite communicates with the best GS by using opportunistic scheduling to maximize the site diversity. More precisely, the paper makes the following specific contributions:

- We focus on the physical layer performance of the downlink optical SatCom, where the best GS is selected among a set of $\mathcal{K}$ sites that are available for communication, to minimize the outage probability and to maximize the ergodic capacity. For this network, we consider an aggregate channel model consisting of turbulence induced fading, and atmospheric attenuation due to Mie scattering and geometrical scattering, and we obtain the instantaneous signal-to-noise ratio (SNR).
- After obtaining the instantaneous SNR, we derive new closed-form outage probability and ergodic capacity expressions to characterize the overall performance of the proposed scheme. We further elaborate the system at high SNR to obtain the overall diversity order.
- We provide two new GS deployment scenarios: ground level deployment and high ground windy weather deployment. We also provide some interesting system design guidelines and consider aperture averaging to mitigate the adverse effects of turbulence induced fading.
- We also obtain the diversity order when a set of satellites form a constellation and communicate with the best GS by using opportunistic scheduling.

---

[1]In laser SatCom, only a small portion of the frequency spectrum can be used due to huge atmospheric losses.

[2]In the proposed setup, we assume that all GSs are connected through fibre-optic wires, and the GS with the highest communication reliability can share the information to the other GSs.
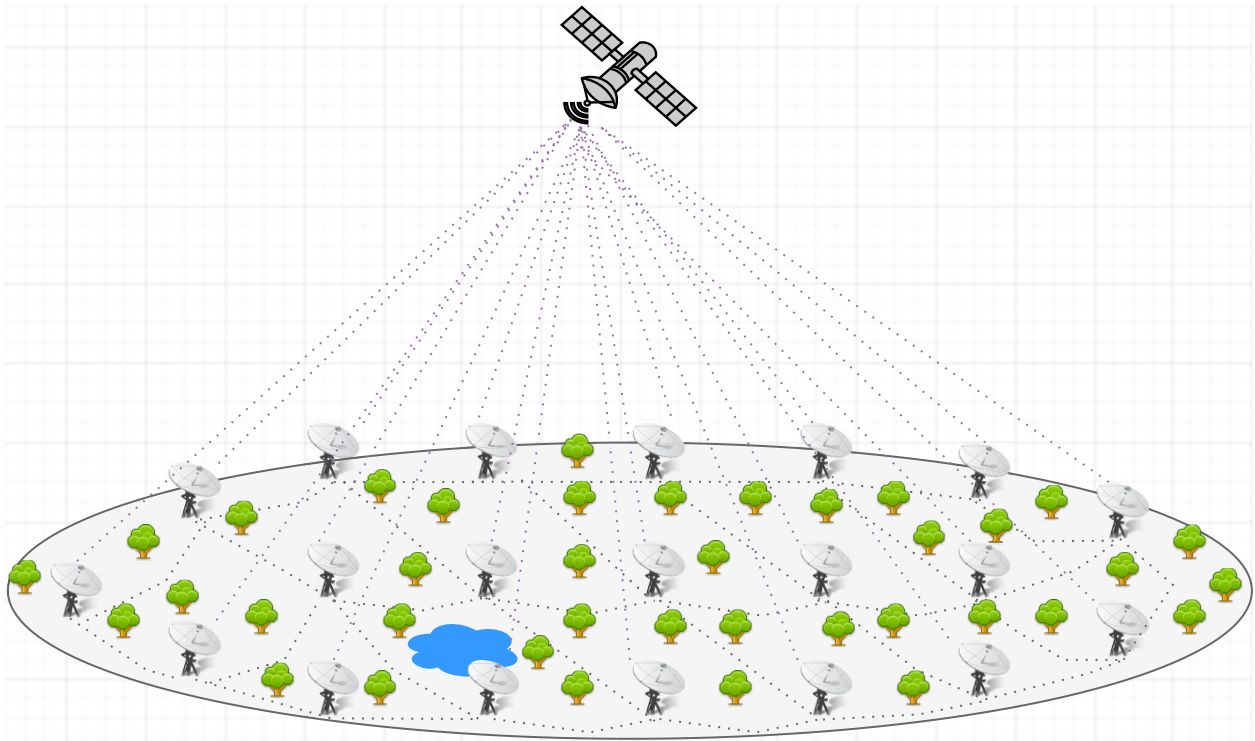
FIGURE 1. Optical downlink SatCom with multiple ground stations.

The remainder of the paper is organized as follows: In Section II, the system model and problem formulation are outlined. In Section III, the outage probability and ergodic capacity analyses are presented, and the overall diversity order of the considered multi-site system is obtained. In Section IV, numerical results are provided, and Section V concludes the paper.

II. SYSTEM MODEL AND PROBLEM FORMULATION

We consider here a downlink optical SatCom where a low Earth orbit (LEO) satellite deployed on a circular orbit at 500 km altitude seeks to communicate with the best GS selected among a set of $\mathcal{K}$ sites that are available for communication, as depicted in Fig. 1. In the proposed model, we assume that all sites are in fixed locations providing perfect LOS connectivity, and the best GS with the highest signal-to-noise (SNR) ratio is selected to enhance the system performance by creating site diversity [25]. Prior to the data transmission, the satellite, which is moving at a speed of 8 km/s, takes aim at the best GS, and the GS is aligned with the incoming beam to compensate for the bore-sight pointing errors. In this setup, the aggregated channel model is taken into consideration which consists of atmospheric attenuation $(I_j^{(a)}\big|_{j=1}^{\mathcal{K}})$ and turbulence induced fading $(I_j^{(t)}\big|_{j=1}^{\mathcal{K}})$. Mathematically speaking, the aggregated channel of the j-th GS can be expressed as [26], [27]

$$I_j = I_j^{(a)} I_j^{(t)}, \qquad (1)$$

and the instantaneous SNR (γ_j) can be expressed as

$$\gamma_j = \frac{P_S}{N_0} I_j^2, \qquad (2)$$

where P_S is the transmitted satellite signal power, and N_0 is the one sided noise power spectral density. The following subsections present the atmospheric attenuation and turbulence induced fading models for the proposed model.

A. ATMOSPHERIC ATTENUATION MODEL

In downlink optical SatCom, two different scattering effects can be observed as the beam propagates to the GS. The first is Mie scattering, which redirects the transmitted signal from its intended direction when the signal wavelength is equal to the diameter of the particles in the medium. The second is geometrical scattering, which causes reflection, refraction, and scattering when the size of the particles in the medium is much greater than the signal wavelength.[3]

1) ATMOSPHERIC ATTENUATION DUE TO MIE SCATTERING

Mie scattering is specified as the primary source of losses in downlink optical SatCom operating between 150 and 375 THz frequencies ($\lambda = 0.8 - 2~\mu$m) and it is largely caused by microscopic particles of water [7, Sec. (3.1)]. The following expression, which can precisely model the Mie scattering effects, is appropriate for GSs located at altitudes

---

[3]It is important to note that Rayleigh scattering may also adversely affect the optical SatCom. However, it can be negligible for systems operating below 375 THz, as per the ITU-R report [7].

between 0 and 5 km above the mean sea level [7]:

$$\rho' = a h_E^3 + b h_E^2 + c h_E + d, \tag{3}$$

where ρ' denotes the extinction ratio, h_E stands for the height of the GS above the mean sea level (km), and a, b, c and d are the wavelength λ (μm)-dependent empirical coefficients, which can be expressed as

$$\begin{aligned}
a &= -0.000545\lambda^2 + 0.002\lambda - 0.0038 \\
b &= 0.00628\lambda^2 - 0.0232\lambda + 0.0439 \\
c &= -0.028\lambda^2 + 0.101\lambda - 0.18 \\
d &= -0.228\lambda^3 + 0.922\lambda^2 - 1.26\lambda + 0.719,
\end{aligned} \tag{4}$$

and the atmospheric attenuation due to Mie scattering $\left(I_j^{(m)} \right)$ can be expressed as

$$I_j^{(m)} = \exp\left(-\frac{\rho'}{\sin(\theta_j)} \right), \tag{5}$$

where θ_j is the elevation angle of the j-th GS.

2) ATMOSPHERIC ATTENUATION DUE TO GEOMETRICAL SCATTERING

Geometrical scattering is used to model the attenuation that is close to the surface of the Earth and is caused by fog or dense clouds. In this model, visibility (V_j), which is an important factor for determining geometrical scattering, can be modeled in terms of liquid water content ($\mathcal{L}_{W_j}$) and cloud number concentration (N_j) as [26]

$$V_j = \frac{1.002}{(\mathcal{L}_{W_j} N_j)^{0.6473}}. \tag{6}$$

These parameters are summarized in Table 1 for various cloud formations. In geometrical scattering, the attenuation can be expressed by using the Beer-Lambert law,

$$I_j^{(g)} = \exp(-\Theta_j L_j), \tag{7}$$

where L_j is the propagation distance, and Θ_j is the attenuation coefficient, which can be expressed as [28, Sect. (3)]

$$\Theta_j = \left(\frac{3.91}{V_j} \right) \left(\frac{\lambda}{550} \right)^{-\psi_j}, \tag{8}$$

where ψ is the particle size related coefficient given according to Kim's model as

$$\psi_j = \begin{cases}
1.6, & V_j > 50 \\
1.3, & 6 < V_j < 50 \\
0.16 V_j + 0.34 & 1 < V_j < 6 \\
V - 0.5 & 0.5 < V_j < 1 \\
0 & V_j < 0.5,
\end{cases} \tag{9}$$

and the atmospheric attenuation $I_j^{(a)}$ for the j-th GS can be expressed as [18]

$$I_j^{(a)} = I_j^{(g)} I_j^{(m)} = \exp(-\sigma_j L_j) \exp\left(-\frac{\rho'}{\sin(\theta_j)} \right). \tag{10}$$

TABLE 1. Geometrical scattering parameters for various types of clouds at 1550 nm.

Cloud type	N (cm^{-3})	$\mathcal{L}_W$ (g/m^{-3})	V (km)
Cumulus	250	1.0	0.0280
Stratus	250	0.29	0.0626
Stratocumulus	250	0.15	0.0959
Altostratus	400	0.41	0.0369
Nimbostratus	200	0.65	0.0429
Cirrus	0.025	0.06405	64.66
Thin cirrus	0.5	3.128×10^{-4}	290.69

B. TURBULENCE INDUCED FADING MODEL

In this paper, the turbulence induced downlink channel experiences an exponentiated Weibull fading channel, where the corresponding probability density function (PDF) and cumulative distribution function (CDF) can be expressed as [29][4]

$$\begin{aligned}
f_{I_j}^{(t)}(I) &= \frac{\alpha_j \beta_j}{\eta_j} \left(\frac{I}{\eta_j} \right)^{\beta_j - 1} \exp\left[-\left(\frac{I}{\eta_j} \right)^{\beta_j} \right] \\
&\quad \times \left(1 - \exp\left[-\left(\frac{I}{\eta_j} \right)^{\beta_j} \right] \right)^{\alpha_j - 1}
\end{aligned} \tag{11}$$

and

$$F_{I_j}^{(t)}(I) = \left(1 - \exp\left[-\left(\frac{I}{\eta_j} \right)^{\beta_j} \right] \right)^{\alpha_j}, \tag{12}$$

where α_j, β_j are the shape parameters and η_j is the scale parameter of the j-th GS. The expressions for α_j, β_j, and η_j can be expressed as [30]

$$\begin{aligned}
\alpha_j &= \frac{7.220 \times \sigma_{I_j}^{2/3}}{\Gamma\left(2.487 \sigma_{I_j}^{2/6} - 0.104 \right)}, \\
\beta_j &= 1.012\left(\alpha \sigma_{I_j}^2 \right)^{-13/25} + 0.142 \\
\eta_j &= \frac{1}{\alpha \Gamma\left(1 + 1/\beta_j \right) g_1(\alpha_j, \beta_j)},
\end{aligned} \tag{13}$$

where $g_1(\alpha_j, \beta_j)$ is the α and β dependent constant variable, which can be written as [30]

$$g_1(\alpha_j, \beta_j) = \sum_{k=0}^{\infty} \frac{(-1)^k \Gamma(\alpha_j)}{k!(k+1)^{1+1/\beta_j} \Gamma(\alpha_j - k)}, \tag{14}$$

and $\sigma_{I_j}^2$ denotes the scintillation index of the j-th GS, which can be given by [31, Sect. (12)]

$$\sigma_{I_j}^2 = \exp\left[\frac{0.49 \sigma_R^2}{\left(1 + 1.11 \sigma_{R_j}^{12/5} \right)^{7/6}} + \frac{0.51 \sigma_{R_j}^2}{\left(1 + 0.69 \sigma_{R_j}^{12/5} \right)^{5/6}} \right] - 1, \tag{15}$$

and the Rytov variance $\sigma_{R_j}^2$ can be expressed as [31, Sect. (12)]

$$\sigma_{R_j}^2 = 2.25 k^{7/6} \sec^{11/6}(\zeta_j) \int_{h_0}^{H} C_{n_j}^2(h)(h - h_0)^{5/6} dh, \tag{16}$$

[4] Throughout the paper, we assume that the height of each GS above the mean sea level is the same. We also assume that all GSs are propagating at the same wavelength. However, the elevation angles and the propagation distances may vary depending on the location of each GS.

where $k = \frac{2\pi}{\lambda}$ is the optical wave number, ζ_j is the zenith angle of the j-th GS, h_0 stands for the height of the GS above ground level, H is the altitude of the satellite, and $C_{n_j}^2(h)$ is the altitude (h) dependent refractive index constant, which can be written as [32]

$$C_{n_j}^2(h) = 8.148 \times 10^{-56} v_{r_j}^2 h^{10} e^{-h/1000} + 2.7$$
$$\times 10^{-16} e^{-h/1500} + C_0 e^{-h/100} \ m^{-2/3}, \quad (17)$$

where $v_{r_j} = \sqrt{v_{g_j}^2 + 30.69 v_{g_j} + 348.91}$ is the r.m.s ground wind speed in m/s, v_{g_j} is the ground wind speed in m/s for the j-th GS, and $C_0 = 1.7 \times 10^{-14}$ is the nominal value of the refractive index constant at ground level. Table 2 summarizes all notations and parameters.

TABLE 2. List of notations and parameters.

Parameter	Definition
D_G	Hard receiver aperture diameter (m)
$\mathcal{K}$	Set of GSs that are available for communication
L	Propagation distance
ζ	Zenith angle
θ	Elevation angle
v_r	Ground r.m.s. wind speed (m/s)
v_g	Ground wind speed (m/s)
h_E	Height of the GS above mean sea level (km)
h	Altitude
H	Altitude of the satellite (m)
h_0	Height of the GS above ground level (m)
ρ_c	Atmospheric correlation width
λ	Wavelength
α, β	Shape parameters of the EW fading
η	Fading severity parameter of the EW fading
k	Optical wave number
V	Visibility (km)
ψ	Particle size related coefficient
N	Cloud number concentration
Θ	Attenuation coefficient
$\mathcal{L}_W$	Liquid water content
σ_R^2	Rytov variance
C_n^2	Refractive index constant
σ_I^2	Scintillation index
γ_{th}	Predefined threshold for acceptable communication quality

C. PROBLEM FORMULATION

This section formulates the GS selection strategy for the proposed setup. In what follows, the GS with the highest instantaneous SNR is selected to maximize the site diversity. Mathematically speaking, it can be formulated as

$$j^* = \arg \max_{1 \le j \le \mathcal{K}} \left[\gamma_j \right], \quad (18)$$

where j^* is the selected GS index. By doing so, outage probability (P_{out}) can be minimized as

$$P_{\text{out}} = \Pr[\gamma \le \gamma_{th}] = \Pr\left[\max_{1 \le j \le \mathcal{K}} (\gamma_j) \le \gamma_{th} \right], \quad (19)$$

where γ_{th} is the predefined threshold for acceptable communication quality. Furthermore, ergodic capacity, which can assess the ergodic channel capacity, can be formulated as [33]

$$\mathcal{C}_{\text{erg}} = \mathbb{E}\left[\log_2 \left(1 + \max_{1 \le j \le \mathcal{K}} (\gamma_j) \right) \right], \quad (20)$$

where $\mathbb{E}[\cdot]$ is the expectation operation. It is important to note that it is almost impossible to find an exact ergodic capacity expression for the proposed scenario by using (20). Therefore, with the aid of Jensen's inequality, we propose two approximate ergodic capacity bounds as given here;

$$\mathcal{C}_{\text{erg}}^{\text{B}_1} \approx \max_{1 \le j \le \mathcal{K}} \mathbb{E}\left[\log_2(1 + \gamma_j) \right], \quad (21a)$$

$$\mathcal{C}_{\text{erg}}^{\text{B}_2} \approx \log_2 \left(\mathbb{E}\left[1 + \max_{1 \le j \le \mathcal{K}} (\gamma_j) \right] \right), \quad (21b)$$

III. PERFORMANCE ANALYSIS

This section derives new closed-form outage probability and ergodic capacity expressions for the proposed system.

A. OUTAGE PROBABILITY ANALYSIS

Outage probability (OP) can be defined as the probability that the SNR will fall below a predefined threshold, γ_{th}, for acceptable communication quality. By substituting (12) into (19), with the aid of (18), the OP can be expressed as

$$P_{\text{out}} = \prod_{j=1}^{\mathcal{K}} \left(1 - \exp\left[-\left(\frac{\gamma_{th}}{\left(\eta_j I_j^{(a)} \right)^2 \bar{\gamma}_j^{(t)}} \right)^{\beta_j/2} \right] \right)^{\alpha_j}, \quad (22)$$

where $\bar{\gamma}_j^{(t)} = \frac{P_S}{N_0} \mathbb{E}\left[\left(I_j^{(t)} \right)^2 \right]$ is the average SNR. By applying the Binomial theorem, and after a few manipulations, a tractable OP expression can be found as

$$P_{\text{out}} = \prod_{j=1}^{\mathcal{K}} \sum_{\rho=0}^{\infty} \binom{\alpha_j}{\rho} (-1)^\rho \exp\left[-\rho \left(\frac{\gamma_{th}}{\left(I_j^{(a)} \eta_j \right)^2 \bar{\gamma}_j^{(t)}} \right)^{\frac{\beta_j}{2}} \right]. \quad (23)$$

To gain further insights about the system behavior, the OP can be analyzed at high SNR. To do so, we first invoke the high SNR assumption of $\exp(-x/a) \approx 1 - x/a$ into (22) as

$$P_{\text{out}}^{\infty} = \prod_{j=1}^{\mathcal{K}} \left[\left(\frac{\gamma_{th}}{\left(\eta_j I_j^{(a)} \right)^2 \bar{\gamma}_j^{(t)}} \right)^{\alpha_j \beta_j/2} \right]. \quad (24)$$

Then, if we express $\bar{\gamma}_j^{(t)} = \kappa_j \bar{\gamma}$, where $\kappa_j |_{j=1}^{\mathcal{K}}$ is constant, after a few manipulations, the above expression can be written as

$$P_{\text{out}}^{\infty} = \prod_{j=1}^{\mathcal{K}} \left[\left(\frac{1}{\left(\eta_j I_j^{(a)} \right)^2 \kappa_j} \right)^{\alpha_j \beta_j/2} \right] \left(\frac{\gamma_{th}}{\bar{\gamma}} \right)^{\sum_{j=1}^{\mathcal{K}} \alpha_j \beta_j/2}. \quad (25)$$

At high SNR, the OP can be expressed as [34]

$$P_{\text{out}}^{\infty} = \mathcal{G}_c (\bar{\gamma})^{-\mathcal{G}_d}, \quad (26)$$

where $\mathcal{G}_c$ determines the shift of the curve in SNR. The diversity order $\mathcal{G}_d$ can be defined as the slope of the OP curve. For the considered multi-site system, $\mathcal{G}_d$ can be obtained as

$$\mathcal{G}_d = \sum_{j=1}^{\mathcal{K}} \alpha_j \beta_j / 2 \qquad (27)$$

If we consider a practical system setup in which a set of $\mathcal{Z}$ satellites form a constellation and communicate with the best GS, which provides the highest SNR, by using opportunistic scheduling in which the best satellite providing best channel characteristics scheduled to communicate with the selected GS depending on the weather conditions, turbulence induced fading and LOS characteristics. In that case, the diversity order of the multi-satellite system can be obtained as

$$\mathcal{G}_d^C = \sum_{z=1}^{\mathcal{Z}} \sum_{j=1}^{\mathcal{K}} \alpha_j \beta_j / 2 \approx \mathcal{Z}\mathcal{K}\alpha\beta/2. \qquad (28)$$

Proof: Please see Appendix.

Furthermore, in this section, we propose two different practical deployment scenarios and investigate the OP performance of the proposed setup when there are $\mathcal{K} = 20$ set of GSs that are available for communication.

1) CASE 1 - GROUND LEVEL DEPLOYMENT SCENARIO

In the first setup, we assume that all GSs are deployed at the ground level ($h_0 = h_E = 0$ m) above the mean sea and ground level, affecting from the nominal ground r.m.s. wind speed, which is $v_g = 2.8$ m/s. Assuming that the average SNR is $\bar{\gamma} = 24$ dB, and $\lambda = 1550$ nm, the OPs that are required for acceptable communication quality ($\gamma_{th} = 7$ dB) can be obtained as given in Case 1, Table 3.

TABLE 3. Outage probabilities for ground level deployment and high ground windy weather deployment scenarios.

Scenario	ζ	N	L_W	Outage probability
Case 1	40°	0.5	3.128×10^{-4}	0.8166
	30°	0.5	3.128×10^{-4}	0.1619
	15°	0.5	3.128×10^{-4}	5.583×10^{-4}
	0°	0.5	3.128×10^{-4}	2.165×10^{-5}
Case 2	40°	0.5	3.128×10^{-4}	0.0986
	30°	0.5	3.128×10^{-4}	2.314×10^{-4}
	15°	0.5	3.128×10^{-4}	2.27×10^{-9}
	0°	0.5	3.128×10^{-4}	1.28×10^{-11}

2) CASE 2 - HIGH GROUND WINDY WEATHER DEPLOYMENT SCENARIO

In the second setup, all GSs are deployed at $h_0 = 1000$ m above from the ground level, and $h_E = 1200$ m above from the mean sea level, where the wind is blowing at a speed of 11.176 m/s. Assuming that the average SNR is $\bar{\gamma} = 24$ dB and $\lambda = 1550$ nm, the OPs that are required for acceptable communication quality can be summarized in Case 2, Table 3. We believe that these deployment scenarios

can be used to provide practical insights about the system architecture, so that a system designer can get a quick idea about the overall system performance.

Table 3 shows the OP results for thin cirrus cloud formations, when the satellite is on a 500 km circular orbit. We can see from the table that, even though the wind speed increases in the high ground deployment, the overall OP performance of the proposed system enhances as both atmospheric turbulence and atmospheric attenuation effects reduces due to lower propagation distance. Furthermore, increasing the zenith angle shows that the GSs are affected by the attenuation and atmospheric turbulence at higher levels. Thereby, keeping the zenith angle small can boost the overall performance and can enhance the overall diversity as can be observed from Fig. 2. Furthermore, when $\mathcal{Z} = 600$ and 1000 constellation of satellites are used, diversity order can be further improved as can be observed from Fig. 3.
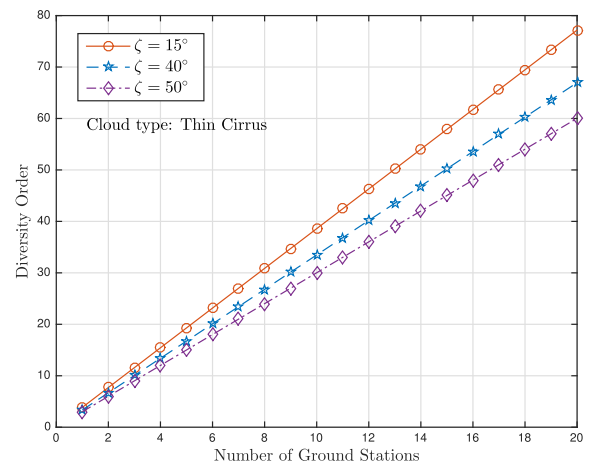
FIGURE 2. Diversity order versus number of ground stations for the ground level deployment scenario.
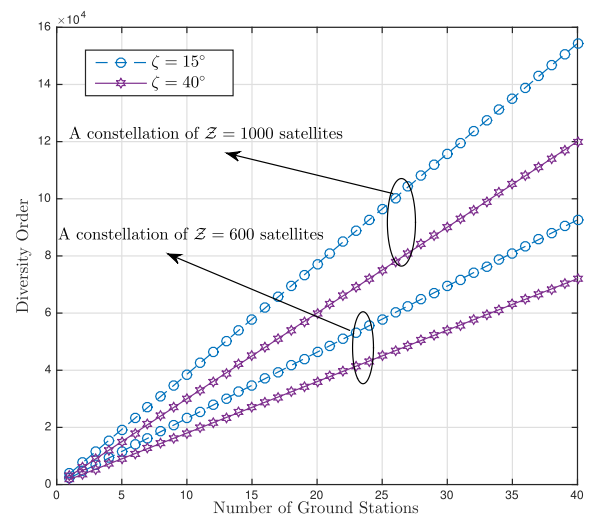
FIGURE 3. Diversity order versus number of ground stations for a constellation of satellites in the ground level deployment scenario.

B. ERGODIC CAPACITY ANALYSIS

1) FIRST APPROXIMATE BOUND ON THE ERGODIC CAPACITY

Ergodic capacity, expressed in bits/channel in use, can be defined with the aid of (21a) as

$$
\mathcal{C}_{\text{erg}}^{B_1} = \log_2(e) \max_{1 \leq j \leq \mathcal{K}} \left\{ \int_0^\infty \frac{1}{1+\gamma} \bar{F}_{\gamma_j}(\gamma) d\gamma \right\}, \quad (29)
$$

where $\bar{F}_{\gamma_j}(\gamma) = 1 - F_{\gamma_j}(\gamma)$ is the complementary CDF of γ_j, which can be given as

$$
\bar{F}_{\gamma_j}(\gamma) = \sum_{\rho=1}^\infty \binom{\alpha_j}{\rho} (-1)^{\rho+1} \exp\left[-\rho \left(\frac{\gamma}{\left(\eta_j I_j^{(a)} \right)^2 \bar{\gamma}_j^{(t)}} \right)^{\frac{\beta_j}{2}} \right], \tag{30}
$$

then, by invoking $\bar{F}_{\gamma_j}(\gamma)$ into (29), $\mathcal{C}_{\text{erg}}$ can be expressed as

$$
\mathcal{C}_{\text{erg}}^{B_1} = \log_2(e) \max_{1 \leq j \leq \mathcal{K}} \left\{ \sum_{\rho=1}^\infty \binom{\alpha_j}{\rho} (-1)^{\rho+1} \int_0^\infty \frac{1}{1+\gamma} \right.
$$

$$
\left. \times \exp\left[-\rho \left(\frac{\gamma}{\left(\eta_j I_j^{(a)} \right)^2 \bar{\gamma}_j^{(t)}} \right)^{\frac{\beta_j}{2}} \right] d\gamma \right\}. \tag{31}
$$

To find the closed-form solution of the above integral, we first use the identity of $\frac{1}{1+\gamma} = G_{1,1}^{1,1}\left[\gamma \left| \begin{matrix} 0 \\ 0 \end{matrix} \right. \right]$, and we can express $\mathcal{C}_{\text{erg}}$ as

$$
\mathcal{C}_{\text{erg}}^{B_1} = \log_2(e) \max_{1 \leq j \leq \mathcal{K}} \left\{ \sum_{\rho=1}^\infty \binom{\alpha_j}{\rho} (-1)^{\rho+1} \int_0^\infty G_{1,1}^{1,1}\left[\gamma \left| \begin{matrix} 0 \\ 0 \end{matrix} \right. \right] \right.
$$

$$
\left. \times \exp\left[-\rho \left(\frac{\gamma}{\Omega_j} \right)^{\frac{\beta_j}{2}} \right] d\gamma \right\}, \tag{32}
$$

where $\Omega_j = \left(I_j^{(a)} \eta_j \right)^2 \bar{\gamma}_j^{(t)}$ and $G_{c,d}^{a,b}\left[\cdot \left| \begin{matrix} \cdot \\ \cdot \end{matrix} \right. \right]$ denotes the Meijer-G function [35, eqn. 07.34.02.0001.01]. By changing variables in the above integration as $\chi = \rho \left(\frac{\gamma}{\Omega_j} \right)^{\frac{\beta_j}{2}}$ and by using the identity of $\exp(-x) = G_{0,1}^{1,0}\left[x \left| \begin{matrix} - \\ 0 \end{matrix} \right. \right]$, the ergodic capacity can be written as

$$
\mathcal{C}_{\text{erg}}^{B_1} = \log_2(e) \max_{1 \leq j \leq \mathcal{K}} \left\{ \sum_{\rho=1}^\infty \binom{\alpha_j}{\rho} (-1)^{\rho+1} \rho^{\frac{\beta_j}{2}} \left(\frac{2\Omega_j}{\beta_j} \right) \right.
$$

$$
\left. \times \int_0^\infty \chi^{\frac{2}{\beta_j}-1} G_{1,1}^{1,1}\left[\Omega_j \left(\frac{\chi}{\rho} \right)^{\frac{2}{\beta_j}} \left| \begin{matrix} 0 \\ 0 \end{matrix} \right. \right] G_{0,1}^{1,0}\left[\chi \left| \begin{matrix} - \\ 0 \end{matrix} \right. \right] d\chi \right\}, \tag{33}
$$

and with the aid of [35, eqn. 07.34.21.0012.01], the closed form solution of the above expression can be

obtained as

$$
\mathcal{C}_{\text{erg}}^{B_1} = \log_2(e) \max_{1 \leq j \leq \mathcal{K}} \left\{ \sum_{\rho=1}^\infty \binom{\alpha_j}{\rho} (-1)^{\rho+1} \rho^{\frac{\beta_j}{2}} \left(\frac{2\Omega_j}{\beta_j} \right) \right.
$$

$$
\left. \times H_{2,1}^{1,2}\left[\Omega_j \rho^{\frac{\beta_j}{2}} \left| \begin{matrix} (0,1), (1-\frac{2}{\beta_j}, \frac{2}{\beta_j}) \\ (0,1) \end{matrix} \right. \right] \right\}. \tag{34}
$$

where $H_{p,q}^{m,n}\left[\cdot \left| \begin{matrix} \cdots \\ \cdots \end{matrix} \right. \right]$ denotes the Fox H-function [36].

2) SECOND APPROXIMATE BOUND ON THE ERGODIC CAPACITY

Another tight bound on the ergodic capacity can be obtained by using (21b). First, recall that

$$
\mathcal{C}_{\text{erg}}^{B_2} \approx \log_2 \left(1 + \mathbb{E}\left[\underbrace{\max_{1 \leq j \leq \mathcal{K}} (\gamma_j)}_{\gamma} \right] \right). \tag{35}
$$

Thereafter, $\mathbb{E}[\gamma]$ can be expressed as

$$
\mathbb{E}[\gamma] = \int_0^\infty (1 - F_\gamma(\gamma)) d\gamma, \tag{36}
$$

where $F_\gamma(\gamma)$ can be obtained very similarly to (23) after changing γ_{th} with γ, and it can be approximately expressed as

$$
F_\gamma(\gamma) \approx \sum_{\rho=0}^\infty \binom{\mathcal{K}\alpha}{\rho} (-1)^\rho \exp\left[-\rho \left(\frac{\gamma_{th}}{\left(I^{(a)} \eta \right)^2 \bar{\gamma}^{(t)}} \right)^{\frac{\beta}{2}} \right]. \tag{37}
$$

By substituting (37) into (36), and after few manipulations, $\mathbb{E}[\gamma]$ can be obtained as

$$
\mathbb{E}[\gamma] = \sum_{\rho=1}^\infty \binom{\mathcal{K}\alpha}{\rho} (-1)^{\rho+1} \rho^{-2/\beta} \bar{\gamma} \left(I^{(a)} \eta \right)^2 \Gamma(1 + 2/\beta). \tag{38}
$$

Finally, substituting (38) into (35), $\mathcal{C}_{\text{erg}}^{B_2}$ can be easily obtained.

C. APERTURE AVERAGING

In downlink optical SatCom, the impact of scintillation can be great enough to limit the performance of GS receivers. To compensate for the impact of scintillation, an important enabler is aperture averaging. In downlink communication, aperture averaging takes place especially when the atmospheric correlation width ρ_{c_j}, which describes the effective diameter of the j-th aperture, is lower than the aperture diameter of the j-th GS (D_{G_j}), i.e, $\rho_{c_j} < D_{G_j}$. In this case, scintillation is spatially averaged over the aperture to reduce the adverse effects of scintillation. For the proposed setup, ρ_{c_j} can be calculated as [31, Sect. (12)]

$$
\rho_{c_j} \approx \sqrt{\frac{45 \times 10^3 \sec(\zeta_j)}{k}}, \quad \sigma_{R_j}^2 \ll 1, \ 0 \leq \zeta_j < 50, \tag{39}
$$

where ρ_{c_j} represents the diameter of the point-like aperture for the GS. For example, when $\zeta_j = 40°$, $\rho_{c_j} \approx 1.204$ cm shows the point-like aperture size for the optical downlink SatCom operating at $\lambda = 1.55$ nm wavelength. In aperture averaging, the aperture diameter dependent scintillation index can be expressed as [31, Sect. (12)]

$$\sigma_{I_j}^2 = 8.7k^{7/6}(H - h_0)^{5/6} \sec^{11/6}(\zeta_j)$$
$$\times \Re\left\{ \int_{h_0}^{H} C_n^2(h) \left[\left(\frac{kD_G^2}{16L} + i\frac{h - h_0}{H - h_0} \right)^{5/6} \right. \right.$$
$$\left. \left. - \left(\frac{kD_{G_j}^2}{16L_j} \right)^{5/6} \right] dh \right\}, \tag{40}$$

where $\Re\{\cdot\}$ represents the real-valued terms. For example, considering $\zeta_j = 40°$, $H = 5 \times 10^5$ m, and thin cirrus cloud formations for the ground level deployment scenario, $D_g = 20$ cm aperture size can boost the overall outage performance from 6.884×10^{-7} to 3.441×10^{-9} at 30 dB average SNR.

IV. NUMERICAL RESULTS

In this section, the theoretical results are first verified by a set of simulations. Then, the ground level deployment scenario is compared with the high ground windy weather deployment scenario in terms of outage probability and ergodic capacity. Finally, aperture averaging is illustrated in terms of outage probability, and important design guidelines are outlined for practical downlink laser SatComs.

In all figures, the parameters are set as $\alpha_j = \alpha$, $\beta_j = \beta$, $\eta_j = \eta$, $I_j^{(a)} = I^{(a)}$, $I_j^{(t)} = I^{(t)}$ $\zeta_j = \zeta$, $\psi_j = \psi$, $C_{n_j}^2(h) = C_n^2(h)$, $\sigma_{I_j}^2 = \sigma_I^2$, $\sigma_{R_j}^2 = \sigma_R^2$ for notational brevity, without losing generality. Furthermore, in the ground level deployment scenario, the parameters are set as $h_0 = h_E = 0$ m, $v_g = 2.8$ m/s, whereas to demonstrate the high ground windy weather scenario, the parameters are set as $h_0 = 1000$ m, $h_E = 1.2$ km, and $v_g = 11.176$ m/s. Finally, the SNR threshold is set to $\gamma_{th} = 7$ dB, and two different cloud forms, cirrus and thin cirrus, are used in the simulations together with three different ζ angles: $\zeta = 15°$, $40°$ and $50°$. All these parameters and values are illustrated in Table 4.

A. VERIFICATIONS OF THE THEORETICAL EXPRESSIONS

Here we verify the theoretical results with the simulations. As we can see in Fig. 4 and 5, the theoretical outage probability results, which are shown with dashed lines, are in good agreement with the marker symbols, which are generated by the simulations. Furthermore, both figures show that the overall outage performance of the proposed scheme can be enhanced remarkably by decreasing the ζ angle as expected. Finally, asymptotic curves, which are depicted with solid lines, show the overall diversity order, which is close to $\mathcal{G}_d = 10\alpha\beta \approx 70$ at both figures.

Fig. 6, on the other hand, illustrates the ergodic capacity performance of the proposed scheme for the high ground

TABLE 4. List of parameters and values.

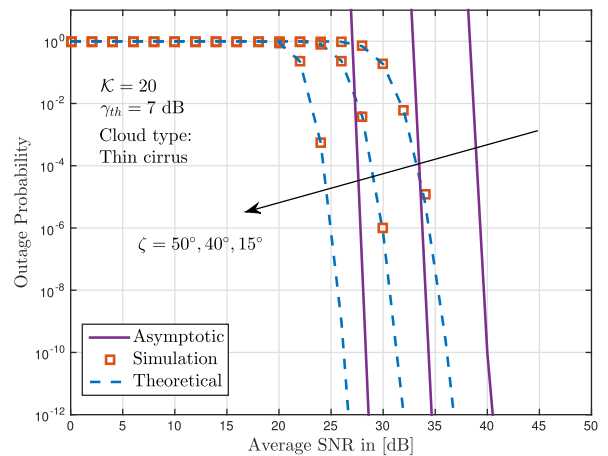| Parameters	Values
$\mathcal{K}$	10, 20
ζ	15°, 40°, 50°
λ	1.55 nm
H	5×10^5 m
h_0	0 m, 1000 m
h_E	0 km, 1.2 km
v_g	2.8 m/s, 11.176 m/s
γ_{th}	7 dB
C_0	1.7×10^{-14}

FIGURE 4. Outage probability performance of the proposed scheme for the ground level deployment scenario.
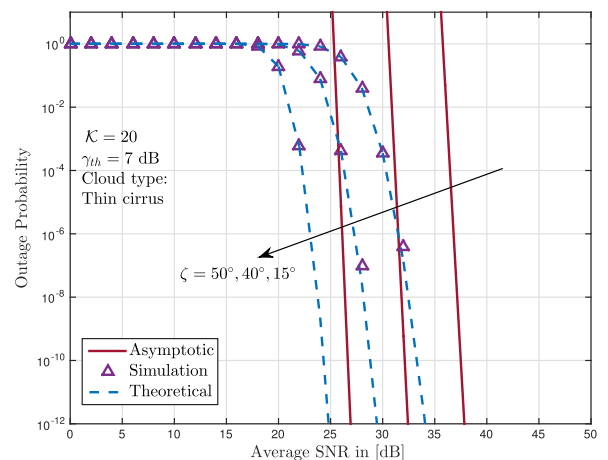

FIGURE 5. Outage probability performance of the proposed scheme for the high ground windy weather deployment scenario.

windy weather deployment scenario.[5] As we can see in the figure, theoretical bound 2, which is shown with solid lines,

---

[5]Theoretical results that are evaluated by using bound 1 (shown with dashed lines) can be easily obtained by using Fox-H function in well-known software programs like MATHEMATICA or MATLAB. However, in a few cases, the Fox-H function may not work properly due to fractional fading severity values. For this reason, numerical integrations are used to verify the correctness of the first bound in certain cases.
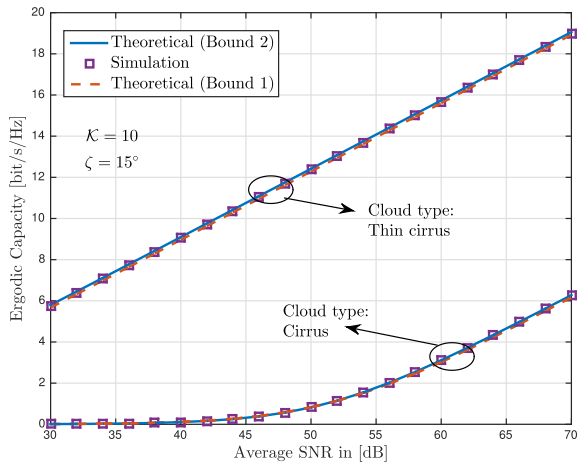
FIGURE 6. Ergodic capacity performance of the proposed scheme for the high ground windy weather deployment scenario.

FIGURE 7. Comparison of ground level deployment with high ground windy weather deployment in terms of outage probability.

provides a tight upper bound, whereas theoretical bound 1, which are indicated with the dashed lines behaves like a tight lower bound with the marker symbols, which are the results of the simulations. Furthermore, thin cloud formations can bring up to 11 bit/s/Hz capacity gain at 50 dB average SNR as the atmospheric attenuation increases due to cirrus cloud formations, and results in losses on the ergodic capacity performance of the proposed scheme.

B. COMPARISON OF HIGH GROUND WINDY WEATHER DEPLOYMENT AND GROUND LEVEL DEPLOYMENT SCENARIOS

Next, the ground level deployment scenario is compared with the high ground windy weather deployment scenario in terms of outage probability and ergodic capacity. Fig. 7 compares both schemes in terms of outage probability. As we can see in the figure, the high ground windy weather scenario outperforms the ground level counterpart both at thin cirrus and cirrus cloud formations, when $\zeta = 15°$. Similarly, Fig. 8 shows the ergodic capacity performance of high ground windy weather deployment and ground level deployment scenarios in terms of zenith angle. As we can see from the figure, high ground windy weather deployment scenario outperforms its counterpart almost for all zenith angles. However, when $\zeta \rightarrow 60°$, the gap between two deployment scenarios are closing and the ergodic capacity performance of the proposed scheme goes to 0. Thereby, in downlink optical SatCom, almost no capacity gain can be obtained when $\zeta > 60°$ as the optical signal is affected more from dense clouds, wind, and atmospheric turbulence induced fading.

C. IMPACT OF APERTURE AVERAGING

This section shows the impact of aperture averaging for the ground level deployment scenario in terms of outage probability. Fig. 9 shows that increasing the receiver aperture diameter up to 20 cm increases the diversity order and enhances the overall performance depending on the zenith
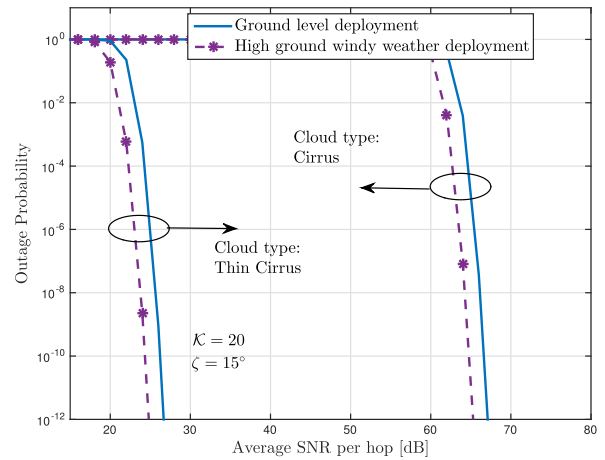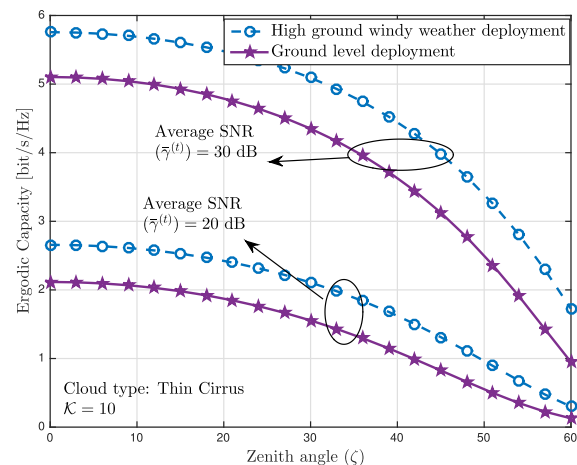

FIGURE 8. Comparison of ground level deployment with high ground windy weather deployment in terms of ergodic capacity.

angle and weather conditions. Also, interestingly, choosing the optimum zenith angle can yield a higher performance gain than aperture averaging.

D. CONSTELLATION OF SATELLITES

This section illustrates the outage probability by considering a constellation of satellites that are communicating with the best GS by using opportunistic scheduling. In Fig. 10, outage probability is depicted for $\zeta = 1000$ constellation of satellites by considering ground level deployment scenario. As can be observed from the figure, a constellation of satellites can bring up to 7 dB average SNR gain at about 10^{-6} outage probability. However, the potential traffic congestion on the inter-satellite communication and the data delivery latency should be taken into consideration.

E. DESIGN GUIDELINES

Finally, we provide some important design guidelines that can be helpful in the design of downlink laser SatCom.
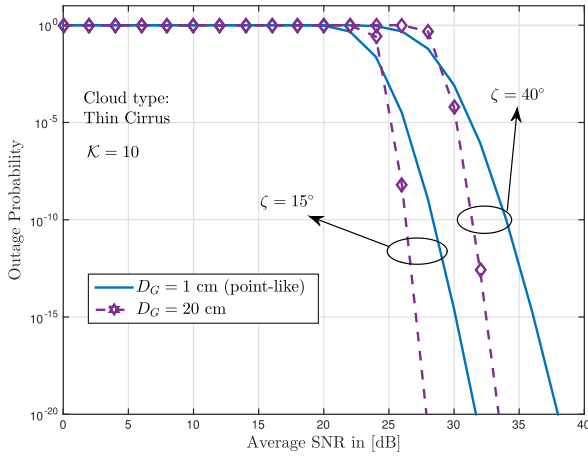
FIGURE 9. The impact of aperture averaging on the ground level deployment scenario in terms of outage probability.
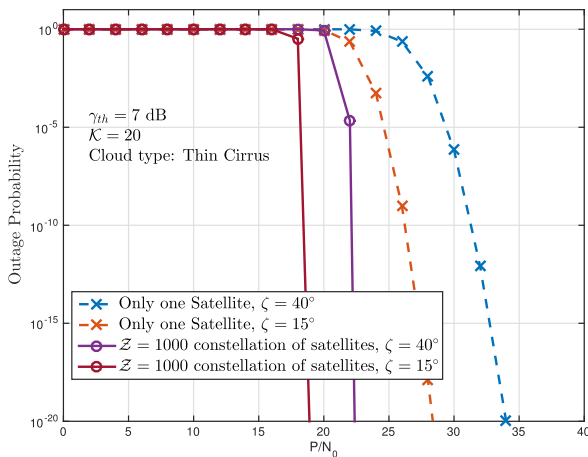

FIGURE 10. Outage probability performance of the proposed scheme for a $\mathcal{Z} = 1000$ constellation of satellites in the ground level deployment scenario.

- The simulations have shown that placing the GS to higher ground reduces the adverse atmospheric conditions and enhances the overall performance. So, the altitude of the GSs is of utmost importance in the design of downlink laser SatComs.
- The zenith angle has a direct impact on the design of downlink laser SatComs as the effect of atmospheric turbulence is much lower when the zenith angle is a small value. For this reason, the zenith angle should be taken into consideration in the design of downlink laser SatCom.
- Aperture averaging can be an important enabler for enhancing the overall performance of the downlink laser SatComs, especially in the presence of adverse weather conditions, and when the zenith angle is higher than $\zeta = 30°$.
- The simulations have shown that less than 10^{-10} outage probability can be achieved at 30 dB when a set of 20 GSs is used. This shows that creating site diversity

through GS selection can be of utmost importance in downlink laser SatComs to enhance the overall performance.

- The simulations have shown that almost no capacity gain can be obtained when the zenith angle is greater than 60° as the system is exposed to higher atmospheric turbulence induced fading and atmospheric attenuation due to increased propagation distance.
- Forming a constellation of satellites can further enhance the performance gain up to 7 dB at 10^{-5} outage probability and diversity order up to a thousand times when the constellations consists of 1000 satellites. However, the potential traffic congestion on the inter-satellite communication and the data delivery latency should be taken into consideration in the design of satellite networks.

V. CONCLUSION

This paper has focused on downlink laser SatComs, where the best GS is selected from among a set of $\mathcal{K}$ candidates to provide fully reliable connectivity and maximum site diversity. For the proposed structure, outage probability and ergodic capacity expressions were derived and asymptotic outage probability was conducted to provide the overall diversity order. Furthermore, we considered two different ground station deployment scenarios and investigated the impact of aperture averaging in terms of outage probability. Finally, important system design guidelines were provided to help in the design of downlink laser SatComs. The results have shown that the altitude of the GS and the zenith angle are of utmost importance in downlink laser SatCom.

APPENDIX
SITE DIVERSITY FOR CONSTELLATION OF SATELLITES

Let us consider that a set of $\mathcal{Z}$ satellites form a constellation and communicating with the best GS which provides the highest signal-to-noise (SNR) with the aid of opportunistic scheduling. In that case, the best GS can be selected as

$$\{z^*, j^*\} = \arg \max_{\substack{1 \leqslant j \leqslant \mathcal{K}, \\ 1 \leqslant z \leqslant \mathcal{Z}}} \left[\gamma_{j,z} \right], \tag{41}$$

where j^* is the selected GS index and z^* is the index of the selected satellite, and the outage probability can be minimized as

$$P_{\text{out}} = \Pr[\gamma \leq \gamma_{th}] = \Pr\left[\max_{\substack{1 \leqslant j \leqslant \mathcal{K}, \\ 1 \leqslant z \leqslant \mathcal{Z}}} (\gamma_{j,z}) \leq \gamma_{th} \right], \tag{42}$$

By substituting (12) into (42) with the aid of (41), with few manipulations, the OP can be expressed as

$$P_{\text{out}} = \prod_{z=1}^{\mathcal{Z}} \prod_{j=1}^{\mathcal{K}} \sum_{\rho=0}^{\infty} \binom{\alpha_{j,z}}{\rho} (-1)^{\rho}$$

$$\times \exp\left[-\rho \left(\frac{\gamma_{th}}{\left(I_{j,z}^{(a)} \eta_{j,z} \right)^2 \bar{\gamma}_{j,z}^{(t)}} \right)^{\frac{\beta_{j,z}}{2}} \right], \tag{43}$$

where $\bar{\gamma}_{j,z}^{(t)} = \frac{P_S}{N_0} \mathbb{E}\left[\left(I_{j,z}^{(t)}\right)^2\right]$ is the average SNR. To obtain the asymptotic behavior of the outage probability, we invoke the high SNR assumption of $\exp(-x/a) \approx 1 - x/a$ into (43) as

$$P_{\text{out}}^{\infty} = \prod_{z=1}^{\mathcal{Z}} \prod_{j=1}^{\mathcal{K}} \left[\left(\frac{\gamma_{th}}{\left(\eta_{j,z} I_{j,z}^{(a)}\right)^2 \bar{\gamma}_{j,z}^{(t)}} \right)^{\alpha_{j,z}\beta_{j,z}/2} \right], \quad (44)$$

and after several manipulations, the diversity order of the considered multi-site system can be obtained as given in (28). Hereto, the proof is completed.

REFERENCES

[1] D. R. Cheruku, *Satellite Communication*. Delhi, India: I.K. International Publishing House Pvt Ltd, 2010.

[2] P. Timothy, W. Bostian, and J. E. Allnutt, *Satellite Communication*. New York, NY, USA: Wiley, 2003.

[3] S. L. Kota, K. Pahlavan, and P. A. Leppänen, *Broadband Satellite Communications for Internet Access*. Norwell, MA, USA: Kluwer Academic Publishers, 2003.

[4] *Starlink*. Accessed: Aug. 20, 2020. [Online]. Available: https://www.starlink.com

[5] *Oneweb*. Accessed: Aug. 20, 2020. [Online]. Available: http://www.oneweb.world

[6] H. Kaushal and G. Kaddoum, "Optical communication in space: Challenges and mitigation techniques," *IEEE Commun. Surveys Tuts.*, vol. 19, no. 1, pp. 57–96, 1st Quart., 2017.

[7] *Prediction Methods Required for the Design of Earth-Space Systems Operating Between 20 THz and 375 THz*, International Telecommunication Union, Recommendation P.1622, 2003.

[8] A. N. Ince, *Digital Satellite Communications Systems and Technologies: Military and Civil Applications*, vol. 186. Springer, Sep. 2012.

[9] D. Giggenbach, B. Epple, J. Horwath, and F. Moll, "Optical satellite downlinks to optical ground stations and high-altitude platforms," in *Advances in Mobile and Wireless Communications*. Springer, Jul. 2008, pp. 331–349.

[10] V. V. Mai and H. Kim, "Mitigation of effects of angle-of-arrival fluctuation and pointing error on airborne free-space optical systems," in *Proc. Opt. Fiber Commun. Conf. (OFC)*, 2019, pp. W2A–40.

[11] D. Agarwal and A. Bansal, "Unified error performance of a multihop DF-FSO network with aperture averaging," *IEEE/OSA J. Opt. Commun. Netw.*, vol. 11, no. 3, pp. 95–106, Mar. 2019.

[12] C. Fuchs and F. Moll, "Ground station network optimization for space-to-ground optical communication links," *IEEE/OSA J. Opt. Commun. Netw.*, vol. 7, no. 12, pp. 1148–1159, Dec. 2015.

[13] M. S. Net, I. D. Portillo, E. Crawley, and B. Cameron, "Approximation methods for estimating the availability of optical ground networks," *J. Opt. Commun. Netw.*, vol. 8, no. 10, pp. 800–812, Oct. 2016.

[14] N. K. Lyras, C. N. Efrem, C. I. Kourogiorgas, and A. D. Panagopoulos, "Optimum monthly based selection of ground stations for optical satellite networks," *IEEE Commun. Lett.*, vol. 22, no. 6, pp. 1192–1195, Jun. 2018.

[15] S. Gong, H. Shen, K. Zhao, R. Wang, X. Zhang, T. D. Cola, and J. A. Fraier, "Network availability maximization for free-space optical satellite communications," *IEEE Wireless Commun. Lett.*, vol. 9, no. 3, pp. 411–415, Mar. 2020.

[16] P. Gopal, V. K. Jain, and S. Kar, "Performance improvement of FSO satellite downlink using aperture averaging and receiver spatial diversity," *IET Optoelectron.*, vol. 10, no. 4, pp. 119–127, Aug. 2016.

[17] K. Li, J. Ma, A. Belmonte, L. Tan, and S. Yu, "Performance analysis of satellite-to-ground downlink optical communications with spatial diversity over gamma–gamma atmospheric turbulence," *Opt. Eng.*, vol. 54, no. 12, pp. 7575–7585, Aug. 2015.

[18] S. Johari and V. Sundharam, "Performance analysis of IM/DD vs. Heterodyne detection techniques of an Earth-satellite FSO link for next generation wireless communication," in *Proc. IEEE 13th Malaysia Int. Conf. Commun. (MICC)*, Nov. 2017, pp. 191–196.

[19] A. Viswanath, V. K. Jain, and S. Kar, "Analysis of Earth-to-satellite free-space optical link performance in the presence of turbulence, beam-wander induced pointing error and weather conditions for different intensity modulation schemes," *IET Commun.*, vol. 9, no. 18, pp. 2253–2258, Dec. 2015.

[20] N. Alshaer, T. Ismail, and M. E. Nasr, "Performance evaluation and security analysis of ground-to-satellite FSO system with CV-QKD protocol," *IET Commun.*, vol. 14, no. 10, pp. 1534–1542, Jun. 2020.

[21] N. Alshaer, T. Ismail, H. Seleem, and M. E. Nasr, "Analysis of beam wander and scintillation in ground-to-satellite FSO system with DPSK," in *Proc. Novel Intell. Lead. Emerg. Sci. Conf. (NILES)*, vol. 1, Oct. 2019, pp. 5–8.

[22] H. D. Le, V. V. Mai, C. T. Nguyen, and A. T. Pham, "Throughput analysis of incremental redundancy hybrid ARQ for FSO-based satellite systems," in *Proc. IEEE 90th Veh. Technol. Conf. (VTC-Fall)*, Sep. 2019, pp. 1–5.

[23] E. Illi, F. El Bouanani, F. Ayoub, and M.-S. Alouini, "A PHY layer security analysis of a hybrid high throughput satellite with an optical feeder link," *IEEE Open J. Commun. Soc.*, vol. 1, pp. 713–731, May 2020.

[24] E. Zedini, A. Kammoun, and M.-S. Alouini, "Performance of multibeam very high throughput satellite systems based on FSO feeder links with HPA nonlinearity," *IEEE Trans. Wireless Commun.*, vol. 19, no. 9, pp. 5908–5923, Sep. 2020.

[25] E. Erdogan, "Joint user and relay selection for relay-aided RF/FSO systems over exponentiated Weibull fading channels," *Opt. Commun.*, vol. 436, pp. 209–215, Apr. 2019.

[26] M. S. Awan, Marzuki, E. Leitgeb, B. Hillbrand, F. Nadeem, and M. S. Khan, "Cloud attenuations for free-space optical links," in *Proc. Int. Workshop Satell. Space Commun.*, Sep. 2009, pp. 274–278.

[27] D. Dubey, Y. K. Prajapati, and R. Tripathi, "Performance enhancement of hybrid-SIM for optical wireless downlink communication with aperture averaging and receiver diversity," *IET Commun.*, vol. 14, no. 18, pp. 3194–3202, Nov. 2020.

[28] Z. Ghassemlooy, W. Popoola, and S. Rajbhandari, *Optical Wireless Communications: System and Channel Modelling With MATLAB*. Boca Raton, FL, USA: CRC Press, 2019.

[29] R. Barrios and F. Dios, "Exponentiated Weibull distribution family under aperture averaging for Gaussian beam waves," *Opt. Exp.*, vol. 20, no. 12, pp. 13055–13064, May 2012.

[30] R. A. Barrios, "Exponentiated Weibull fading channel model in free-space optical communications under atmospheric turbulence," Ph.D. dissertation, Dept. Signal Theory Commun., Univ. Politècnica de Catalunya (UPC), Barcelona, Spain, May 2013.

[31] L. Andrews and R. Phillips, *Laser Beam Propagation Through Random Media* (SPIE Press Monograph). Bellingham, WA, USA: SPIE, 2005.

[32] *Propagation Data Required for the Design of Earth-Space Systems Operating Between 20 THz and 375 THz*, International Telecommunication Union, Recommendation P.1621-1, 2019.

[33] J. Choi and B. L. Evans, "Analysis of ergodic rate for transmit antenna selection in low-resolution ADC systems," *IEEE Trans. Veh. Technol.*, vol. 68, no. 1, pp. 952–956, Jan. 2019.

[34] Z. Wang and G. B. Giannakis, "A simple and general parameterization quantifying performance in fading channels," *IEEE Trans. Commun.*, vol. 51, no. 8, pp. 1389–1398, Aug. 2003.

[35] *From Wolfram Research: The Mathematical Functions Site*. Accessed: Jun. 18, 2020. [Online]. Available: http://functions.wolfram.com

[36] A. M. Mathai, R. K. Saxena, and H. J. Haubold, *The H-Function: Theory and Applications*. Springer, 2009.

EYLEM ERDOGAN (Senior Member, IEEE) was a Postdoctoral Fellow with the Department of Electrical Engineering, Lakehead University, Thunder Bay, ON, Canada, from March 2015 to September 2016, and a Visiting Professor with Carleton University, Ottawa, ON, Canada, during Summer 2019. He is currently an Associate Professor with the Department of Electrical and Electronics Engineering, Istanbul Medeniyet University. His research interests include wireless communications, performance analysis of cooperative relaying in cognitive radio networks, unmanned aerial vehicle communications and networks, free space optical communications, and optical satellite networks.

IBRAHIM ALTUNBAS (Senior Member, IEEE) was a Visiting Researcher with Texas A&M University, College Station, TX, USA, in 2001. He was a Postdoctoral Fellow and a Visiting Professor with the University of Ottawa, Ottawa ON, Canada, in 2002 and 2015 Summer, respectively. He is currently a Professor with the Electronics and Communication Engineering Department, Istanbul Technical University. His current research interests include spatial modulation, non-orthogonal multiple access, physical layer security, drone communications, and reconfigurable intelligence surface-based communication.

GUNES KARABULUT KURT (Senior Member, IEEE) received the B.S. degree (Hons.) in electronics and electrical engineering from Boğazi çi University, Istanbul, Turkey, in 2000, and the M.A.Sc. and Ph.D. degrees in electrical engineering from the University of Ottawa, Ottawa, ON, Canada, in 2002 and 2006, respectively. From 2000 to 2005, she was a Research Assistant with the CASP Group, University of Ottawa. From 2005 to 2006, she was with TenXc Wireless, Canada. From 2006 to 2008, she was with Edgewater Computer Systems Inc., Canada. From 2008 to 2010, she was with Turkcell Research and Development Applied Research and Technology, Istanbul. Since 2010, she has been with Istanbul Technical University, where she currently works as a Professor. She is also an Adjunct Research Professor with Carleton University. She is a Marie Curie Fellow. She currently serving an Associate Technical Editor (ATE) for IEEE *Communications Magazine*.

MICHEL BELLEMARE received the B.Eng. degree in communications engineering from the Université de Sherbrooke, Sherbrooke, QC, Canada, in 1986. He is currently a Space Systems Architect with MDA Corporation, Sainte-Anne-de-Bellevue, QC, Canada. He has gained experience in terrestrial and space wireless communications in various companies, such as Nortel Networks, Ultra Electronics, SR Telecom, and so on.

GUILLAUME LAMONTAGNE received the B.Eng. and M.Eng. degrees from the École de Technologie Supérieure (ÉTS), Montréal, QC, Canada, in 2007 and 2009 respectively. His experience in satellite communications started through internships and research activities with the Canadian Space Agency (CSA), in 2005, and the Centre national d'études spatiales (Cnes), France, in 2006 and 2008. He joined MDA in 2009 and held various communication systems engineering and management positions before being appointed as the Director of Technology, Payloads, in 2019. Through this role, he is leading MDA's Research and Development activities for satellite communications as well as establishing the related long term development strategy.

HALIM YANIKOMEROGLU (Fellow, IEEE) received the B.Sc. degree in electrical and electronics engineering from the Middle East Technical University, Ankara, Turkey, in 1990, and the M.A.Sc. degree in electrical engineering and the Ph.D. degree in electrical and computer engineering from the University of Toronto, Toronto, ON, Canada, in 1992 and 1998, respectively. He is currently a Professor with the Department of Systems and Computer Engineering, Carleton University, Ottawa, ON, Canada. His collaborative research with industry has resulted in 37 granted patents. His research interests include many aspects of 5G/5G+ wireless networks. He is a Fellow of the Engineering Institute of Canada (EIC) and the Canadian Academy of Engineering (CAE). He is a Distinguished Speaker for the IEEE Communications Society and the IEEE Vehicular Technology Society.

● ● ●